Non-Fourier Encoded Parallel MRI Using Multiple Receiver Coils

Dimitris Mitsouras[1], W. Scott Hoge[2], Frank J. Rybicki[2], Walid E. Kyriakos[2], Alan Edelman[3], Gary P. Zientara[2]

This paper describes a general theoretical framework combining non-Fourier spatially encoded MR imaging with multi-channel acquisition parallel MR imaging. The two spatial encoding mechanisms are physically and analytically separable, allowing non-Fourier encoding to be expressed as complementary to the inherent encoding imposed by RF receiver coil sensitivities. Consequently, the number of non-Fourier spatial encoding steps necessary to fully encode a FOV is reduced. Furthermore, by casting the FOV reduction of parallel imaging techniques as a dimensionality reduction of the *k*-space that is non-Fourier encoded, a speedup of each digital non-Fourier spatial excitation may be obtained in addition to imaging acceleration. Images acquired at speedup factors of 2x to 8x using a 4-element RF receiver coil array demonstrate use of the framework and the efficiency afforded by it.

Key words: Non-Fourier spatial encoding; Parallel Imaging; SENSE; SMASH; Space-RIP; Adaptive MRI; Dynamic Acquisitions

INTRODUCTION

A wide variety of MR imaging techniques available today aim to increase signal acquisition efficiency. A recent addition to the fast imaging methods toolbox are multi-channel parallel data acquisition (P-MRI) methods, characterized by multiple RF receiver coils and associated RF receiver electronics. P-MRI methods such as SMASH (1), SENSE (2) and Space-RIP (3) offer improved temporal and/or spatial resolution and are rapidly becoming a prominent focus of research and MR scanner design, motivated primarily by the numerous clinical imaging applications that require both high speed and resolution, such as cardiac imaging. Each P-MRI method uses a unique reconstruction scheme which exploits the independence of the spatial sensitivity profiles of the RF coils. P-MRI methods have been successfully combined with other fast acquisition methods, offering further improvements. For example, the UNFOLD method for increasing temporal resolution was recently applied to parallel coil acquisition (4), (5), and non-Cartesian SENSE (6) renders the use of the SENSE P-MRI reconstruction technique compatible with complicated *k*-space trajectories, such as spiral imaging, that are typically used for fast MRI.

Non-Fourier (NF) imaging partially encodes the field-of-view (FOV) by employing non-sinusoidal spatial encoding profiles induced via RF excitation. NF encoding has been used for effective inter-view motion compensation (7), volume imaging of the heart (8), increasing effective relaxation times (7), or, imaging with multiple resolutions along the phase-encode and slice-select dimensions (MURPS) (9). NF spatial encoding can be derived from well-known fixed mathematical basis sets, such as Hadamard (10) and Wavelet (7) bases that are popular in signal processing. It can also be derived dynamically to adapt to the changing contents of the FOV (11), (12). Such dynamic adaptive *near-optimal* NF encoding exploits *a priori* information about the imaged sample in order to further reduce image acquisition times, for example via Wavelet or Singular Value Decomposition (SVD) encoding (13), (11). NF encoding can compact the acquired signal space while maximizing the amount of pertinent image information that is captured.

We develop a method to combine P-MRI with NF spatial encoding methods in a manner that enables advantages in addition to the temporal resolution improvement associated with parallel acquisition. Modus operandi of P-MRI methods is a *k*-space subsampling scheme resulting in the superposition of multiple regions of the FOV. This is exploited to reduce the NF encoding burden by encoding all aliases simultaneously: each superimposed portion is NF encoded identically. Combination of P-MRI "decoding" techniques with NF encoding enables the speedup factors associated with each method to multiply thereby yielding greatly reduced image acquisition times. Furthermore, just as aliased images result by skipping acquisition of *k*-space samples, aliased RF spatial excitations result by skipping excitation *k*-space samples. This enables a reduction of the length of the digital RF spatial encoding pulses by a factor up to the speedup factor of the P-MRI method.

Below, we extend the general digital NF encoding methodology introduced by Panych et. al. (14) to include the spatial encoding induced by non-uniform coil sensitivities. This is then used to construct a composite digital non-Fourier system response that includes signal from multiple RF receiver coils. Finally this composite system response is shown to enable NF spatially encoded P-MRI, termed NF*P. Finally, the methods presented aim to materialize the digital NF*P encoding methodology while results demonstrate the combination.

THEORY

In Fourier-basis imaging, the received MR signal can be described by the equation

$$s(\mathbf{k}) = \int_V \rho(\mathbf{r}) e^{i2\pi \mathbf{k}\cdot\mathbf{r}} d\mathbf{r}, \qquad [1]$$

where $\rho(\mathbf{r})$ is the excited spin density function throughout the sample volume V, weighted by various imaging factors (e.g., relaxation terms, hardware characteristics etc.), $\mathbf{r}$ is the spatial position of the spins, and $\mathbf{k}$ is a reciprocal spatial term corresponding to the applied gradients (see e.g., (15)).

To develop the theory, we consider a simple 2D spin-echo experiment. Letting the readout, phase encode, and slice-select gradients as G_x, G_y and G_z respectively, Eq. [1] is represented as

$$s(k_y, k_x) = \int_{-\alpha}^{\alpha} \iint \rho(x, y, z) e^{i2\pi(k_x x + k_y y)} dx\, dy \quad dz \qquad [2]$$

where 2α is the thickness of the excited slice. In the spin-echo experiment slice selection is additionally performed by the slice-selective 180° refocusing RF pulse.

Given the desired FOV, manipulation of the readout and phase encoding gradients produces samples at $k_x = n\Delta k_x$ and $k_y = m\Delta k_y$ steps through *k*-space, such that $-N/2 < n \leq N/2$, $-M/2 < m \leq M/2$. The MR system response matrix can then be defined by placing these samples in the M-by-N *k*-space matrix $\mathbf{S}$, with readout samples placed along the columns. Inverse Fourier transformation (denoted $\mathcal{F}^{-1}\{\cdot\}$) of this matrix reconstructs the weighted spin density image of the slice, $\mathbf{R} = \mathcal{F}^{-1}\{\mathbf{S}\}$ with the well known approximation errors (16).

Digital Non-Fourier Spatial Encoding

The digital NF spatial encoding methodology (14) replaces the initial slice-selective RF pulse with a spatial excitation profile along the phase-encode direction, while eliminating the phase encode gradient of the

[1]Department of Electrical Engineering and Computer Science, Lab for Computer Science, Massachusetts Institute of Technology, Cambridge, Massachusetts.

[2]Department of Radiology, Brigham and Women's Hospital and Harvard Medical School, Boston, Massachusetts.

[3]Department of Applied Mathematics, Lab for Computer Science, Massachusetts Institute of Technology, Cambridge, Massachusetts.

[0]Grant Sponsor: NIH NCI R01-CA78299; Grant Sponsor: NIH NCI P01-CA67165; Grant Sponsor: BWH Research Council Interdisciplinary Seed Grant; Grant Sponsor: Edgerly Science Partnership Award (A.E. and G.Z.); Grant Sponsor: Oxygen Alliance grant.

typical sequence (c.f. Fig. 1). Slice selection is performed exclusively by the 180° refocuser although a 2D z-y spatial excitation that additionally selects a slice along z can be employed. We define the RF pulse by the envelope $p(t) = \sum_{m=1}^{M} p_m \Pi((t - m\Delta t)/\Delta t)$, where $\Pi(t)$ is zero except in the interval $0 \leq t < 1$. If the RF pulse is low flip ($\theta(\mathbf{r}) < 30^\circ$ (15)) and is applied during a gradient G_y of duration $M\Delta t$ followed by a rephasing gradient of half area, each constituent "hard pulse" p_m excites some magnetization that remains undisturbed by subsequent hard pulses and freely precesses under the influence of the remaining gradients. With no other y gradient applied, each hard pulse can be thought of as generating the Fourier mode $k_m = (1/2M - m)G_y\Delta t$, but, scaled by the complex value p_m. In the low flip-angle approximation, the signal received due to this arbitrary RF pulse is a superposition of the individual hard pulse contributions (14):

$$a(\mathbf{p}, k_x) = \int_{-a}^{a} \iint \rho(x, y, z) \left(\sum_{m=1}^{M} p_m e^{i2\pi k_m y} \right) \times e^{i2\pi k_x x} dx\, dy\, dz \quad [3]$$

$$= \sum_{m=1}^{M} p_m s(k_m, k_x), \quad [4]$$

where $\mathbf{p}$ is a row vector containing the p_m, i.e., $\mathbf{p} = (p_1, \cdots, p_M)$. With sufficient gradient strength, the k_m can precisely reflect the phase encodes k_y of the Fourier experiment. The Fourier transform term enclosed in parentheses in Eq. [3] is the spatial profile of transverse magnetization generated by the RF pulse, $\tilde{p}(y) \approx \mathcal{F}\{\mathbf{p}\}$. The sampled signal is then most accurately described as the projection of this spatial profile of magnetization onto the readout axis. Equation [4] recasts the NF signal equation of Eq. [3] as a linear combination of the typical Fourier modes of the sample, weighted by the entries in the RF encoding vector $\mathbf{p}$.

Equation [4] can be rewritten in matrix-vector form as $\mathbf{a} = \mathbf{pS}$ (14), when the length-M input vector $\mathbf{p}$ describes the RF excitation waveform, $\mathbf{a}$ is the length-N output "response" vector of sampled data, and $\mathbf{S}$ is again the M-by-N system response (*k*-space) matrix corresponding to the spin distribution. One may now consider MR image encoding using arbitrary RF inputs $\mathbf{p}$. Given an arbitrary invertible matrix $\mathbf{P}$, we can use its rows as the RF pulse of each repetition of the NF encoded experiment. Collecting the sampled responses into the rows of the matrix $\mathbf{A}$, the NF MR imaging process is expressed as (14):

$$\mathbf{A} = \mathbf{PS}, \quad [5]$$

which yields the *k*-space matrix by using an appropriate inverse:

$$\mathbf{S}_{\text{est}} = \mathbf{P}^{\dagger}\mathbf{A}. \quad [6]$$

Inverse Fourier transformation of $\mathbf{S}_{\text{est}}$ yields the desired image.

Based on Eq. [6], Hadamard, Wavelet and Singular Value Decomposition (SVD) based input vector sets have been studied (10), (7), (17) and used (8), (9) for MRI. For example, Hadamard encoding derives the matrix $\mathbf{P}$ from the M-by-M Hadamard matrix $\mathbf{H}_M$ (c.f. Eq. [17]) whose rows then become the spatial excitations $\tilde{p}(y)$. Wavelet encoding similarly derived from the M-by-M Haar wavelet matrix (18) is another example. The SVD method chooses a reduced set of $K \leq M$ input vectors

$$\mathbf{P}_{\text{SVD}} = \begin{bmatrix} \mathbf{p}_1 \\ \vdots \\ \mathbf{p}_K \end{bmatrix}, \quad [7]$$

based on maximizing the power of $\mathbf{S}$ that is captured by these K vectors. The SVD of an estimate of $\mathbf{S}$ (or of a reference image $\mathbf{R}$, since the two are related by the unitary Fourier transform) yields a near optimal set of such vectors. This basis minimizes the mean squared error function $e = \|\mathbf{S} - \mathbf{S}_{\text{est}}\|_F^2 = \|\mathbf{S} - (\mathbf{P}_{\text{SVD}}^H \mathbf{P}_{\text{SVD}})\mathbf{S}\|_F^2$, over any possible set of K vectors, provided the FOV contents are unchanged. The K-by-M matrix $\mathbf{P}_{\text{SVD}}$ completes encoding of $\mathbf{S}$ in K repetitions of the pulse sequence, thereby yielding a speedup of M/K compared to *oblivious* (i.e., fixed basis) encoding modalities such as Fourier or Hadamard encoding that do not exploit *a priori* information about the imaged sample. However, the reconstructed image retains an intrinsic resolution of M along the NF encoded direction (e.g., along k_y).

Non-Fourier Excitation with Parallel Receiver Coils

To merge NF encoding with parallel receiver coil signal acquisition, the signal equation, Eq. [1], is augmented with an additional term describing the spatial sensitivity weighting $W_l(\mathbf{r})$ of receiver coil l, of a set of L coils. The signal acquired in each coil is then described by (1), (2), (19):

$$s_l(\mathbf{k}) = \int_V W_l(\mathbf{r})\rho(\mathbf{r})e^{i2\pi\mathbf{k}\cdot\mathbf{r}}d\mathbf{r}. \quad [8]$$

Discretization of Eq. [8] following the 2D example describes the *k*-space matrix sampled by each coil as

$$\mathbf{S}_l = \mathcal{F}\{\mathbf{W}_l \circ \mathbf{R}\}, \quad [9]$$

where $\mathbf{R}$ is the weighted spin density image of the slice as before, and, $\mathbf{W}_l$ is the discretized form of the coil sensitivity, $W_l(\mathbf{r})$. Here, the *k*-space system response matrix $\mathbf{S}_l$ is derived from an element-by-element-wise product, (denoted $\circ$), of the discretized spatial sensitivity profile of coil l and spatial spin distribution.

In Fourier encoded parallel imaging, a reduction in acquisition time is achieved by acquiring only a subset of lines of *k*-space while sampling the signal using multiple coils with different spatial sensitivities. We represent this with a sparse matrix $\mathbf{D}$ derived from the M-by-M identity matrix, $\mathbf{I}_{M\times M}$. For Fourier-basis imaging, each row of $\mathbf{D}$ corresponds to a repetition of the sequence (i.e., phase encode step). The column of $\mathbf{D}$ that the one appears in represents the particular phase encode step k_y that is sampled at that repetition. The ratio of number of columns to rows in $\mathbf{D}$ indicates the P-MRI speedup factor. The signals sampled by coil l in a parallel imaging experiment can then be compactly expressed using $\mathbf{D}$ as

$$\mathbf{S}_l^{(f)} = \mathbf{D}\left(\mathcal{F}\{\mathbf{W}_l \circ \mathbf{R}\}\right), \quad [10]$$

where the superscript (f) denotes acquisition at a speedup of f. The matrix $\mathbf{D}$ then has dimensions M/f-by-M.

Originally, SMASH (1) and SENSE (2) required that $\mathbf{D}$ be derived by regular downsampling of the identity matrix. For example, for a speedup factor of two, $\mathbf{D}$ contains only every second row of $\mathbf{I}$, corresponding to skipping every second phase encode. Space-RIP, and subsequent adaptations of SMASH and SENSE, can reconstruct the image given any arbitrary set of M/f rows of the identity matrix (i.e., given any arbitrary reduced set of phase encode lines).

Regardless of which P-MRI method is used, once the downsampling matrix $\mathbf{D}$ for a speedup of f is chosen, the weighted *k*-space matrix $\mathbf{S}_l^{(f)}$ is obtained from a number of coils $l = 1, \cdots, L$ with $L \geq f$, each with differing (linearly independent) sensitivity, providing independent information about the sample. Each *k*-space matrix obtained represents the f-fold-subsampled sensitivity-weighted spin density image seen by the respective coil. The ensemble of matrices are then used with the P-MRI method to produce the full FOV *k*-space or image. The goal of any spatial encoding method is to produce precisely these $\mathbf{S}_l^{(f)}$, or accurate estimates thereof, so that parallel reconstruction can then be applied to produce the image.

To enable the potential of NF encoding with P-MRI, we further augment Eq. [8] with a spatially selective term $\tilde{p}(\mathbf{r})$ that, as before, corresponds to the spatial RF excitation $\mathbf{p}$. The equation describing the received signal thus becomes (20):

$$a_l(\mathbf{k},\mathbf{p}) = \int_V W_l(\mathbf{r})\rho(\mathbf{r})\tilde{p}(\mathbf{r})e^{i2\pi\mathbf{k}\cdot\mathbf{r}}d\mathbf{r}. \quad [11]$$

Discretization of this expression, as for the 2D example with the uniform sensitivity coil (c.f. Eq. [4]), results in a linear equation relating the signal acquired by coil l and the discrete RF input as

$$\mathbf{a}_l = \mathbf{p}\mathbf{S}_l = \mathbf{p}(\mathcal{F}\{\mathbf{W}_l \circ \mathbf{R}\}). \quad [12]$$

We note that the goal of the *parallel* NF imaging experiment is to produce the matrix $\mathbf{S}_l^{(f)}$ of Eq. [10]. Therefore, the RF pulse only needs to encode those Fourier modes (i.e., those necessary for P-MRI reconstruction). We may thus craft the spatially selective RF excitation to only encodes those modes. This is done by using the subsampling matrix $\mathbf{D}$. Noting that this matrix operates on the left, it is the vector $\mathbf{p}^{(f)} = \mathbf{p}\mathbf{D}^T$ of length M/f, that captures precisely the selected Fourier modes. The signal produced when using this encoding vector only contains those Fourier modes necessary for parallel reconstruction:

$$\mathbf{a}_l^{(f)} = \mathbf{p}^{(f)}\mathbf{D}(\mathcal{F}\{\mathbf{W}_l \circ \mathbf{R}\}) = \mathbf{p}^{(f)}\mathbf{S}_l^{(f)}. \quad [13]$$

The physical analogue of the spatial excitation $\mathbf{p}^{(f)}$ is revealed by expanding Eq. [13] to obtain $\mathbf{a}_l^{(f)} = \mathbf{p}\ \mathbf{D}^T\mathbf{D}\ (\mathcal{F}\{\mathbf{W}_l \circ \mathbf{R}\})$. In particular, the composite matrix $\mathbf{D}^T\mathbf{D}$ is simply a projection matrix. When applied to the full FOV excitation $\mathbf{p}$, the projection $\mathbf{p}\mathbf{D}^T\mathbf{D}$ has the effect of replacing with zeros those elements of $\mathbf{p}$ that correspond to Fourier modes of the sample that are not necessary for P-MRI reconstruction. When $\mathbf{D}$ is the regularly downsampled identity, projection amounts to replacing with zeros $f-1$ elements following each element of the vector that is retained. The spatial domain analogue of this projection is given by the Fourier transform $\tilde{p}^{(f)}(y) \approx \mathcal{F}\{\mathbf{p}\mathbf{D}^T\mathbf{D}\}$, which describes a function that is repeated f times over the FOV. That is, the spatial encoding function is an f-fold aliased function.

The non-Fourier Parallel Imaging System Response Matrix

When L coils are used to sample the signal resulting from the application of the spatially selective RF pulse $\mathbf{p}^{(f)}$, the individual coil responses of Eq. [13] can be combined by concatenation into a single vector as

$$\mathbf{a}^{(f)} \equiv \left[\mathbf{a}_1^{(f)}|\cdots|\mathbf{a}_L^{(f)}\right] = \mathbf{p}^{(f)}\left[\mathbf{S}_1^{(f)}|\cdots|\mathbf{S}_L^{(f)}\right] \equiv \mathbf{p}^{(f)}\mathbf{S}^{(f)}, \quad [14]$$

where the symbol "|" denotes matrix or vector concatenation as appropriate. Equation [14] effectively reveals a composite *k*-space system response matrix, $\mathbf{S}^{(f)}$, capturing the subsampled output from multiple coils in a concise fashion. This composite response matrix has dimensions M/f-by-LN, given the number of coils L, the size of the desired *k*-space information (M-by-N), and the P-MRI speedup factor f. When the input RF encoding vector $\mathbf{p}^{(f)}$ of length M/f is applied, the ensemble of coils produce the composite response $\mathbf{a}^{(f)}$ of length LN. Fundamentally then, Eq. [14] allows one to apply any NF encoding method in the same fashion as the single uniform sensitivity coil digital NF encoding methodology.

The difference of this P-MRI enabled composite system response matrix is that its column space is intrinsically smaller. For example, in order to produce a target resolution of M along the NF encoded dimension using a P-MRI speedup of f and full encoding of the *k*-space, one can use the rows of an arbitrary M/f-by-M/f invertible matrix $\hat{\mathbf{P}}$ for the set of excitations, reflecting the P-MRI efficiency. For reduced basis adaptive imaging, the encoding matrix $\hat{\mathbf{P}}$ is K-by-M/f, where $K \leq M/f$, reflecting the additional NF efficiency. In every case, the sampled signals form the matrix

$$\mathbf{A}^{(f)} = \hat{\mathbf{P}}\mathbf{S}^{(f)} \quad [15]$$

of size K-by-LN, $K \leq M/f$. NF inversion of Eq. [15] yields the individual coil subsampled *k*-space matrices as

$$\mathbf{S}_{\text{est}}^{(f)} = \hat{\mathbf{P}}^{\dagger}\mathbf{A}^{(f)}. \quad [16]$$

The matrix $\mathbf{S}^{(f)}$ can be separated by reversing the concatenation, and its constituents can be used with the P-MRI algorithm of choice to reconstruct the full M-by-N image of the FOV.

METHODS

Equipment

Waveform generation and image reconstruction was performed using the MATLAB language interpreter (The Mathworks,Natick, MA) on an Intel-based workstation. All experiments were performed using a commercial four-element phased array cardiac receiver on a 1.5T GE Signa Horizon LX EchoSpeed MR imager (GE Medical Systems, Milwaukee, WI). The scanner is equipped with 4 G/cm gradient coils at 14.9 G/cm/msec maximum slew rate, while maximum B_1 is 250 mG. None of these limits are reached for the sequence used (c.f. Fig. 1). In general, NF*P imaging acceleration is affected by these limits just as P-MRI methods are. RF pulse acceleration is however highly dependent on hardware limits as well as the specific pulse. Variable rate selective excitation (VERSE) (21) encapsulates these limitations, while reduction of the number of hard pulses by NF*P can reduce RF pulse requirements within VERSE.

Non-Fourier Encoding Pulse Sequence

A simple NF encoding spin-echo pulse sequence (22) was used to excite the spatial encoding profiles as shown in Fig. 1. Here, G_x, G_y, and G_z, correspond to the readout, spatially selective encoded, and slice-select (for the 180° pulse) gradients respectively. Typical low flip ($\theta \simeq 30^\circ$) unoptimized RF pulses (i.e., not VERSE'd) require Δt in the range of 16 to 20 μsec. Accordingly, an RF pulse designed for a resolution of $M = 256$ requires $M\Delta t = 5.12$ msec, compared to the standard 3.2 msec 90° slice-select pulse used by commercial sequences on our system. A P-MRI speedup of f reduces the length of this NF excitation pulse to $M\Delta t/f$.

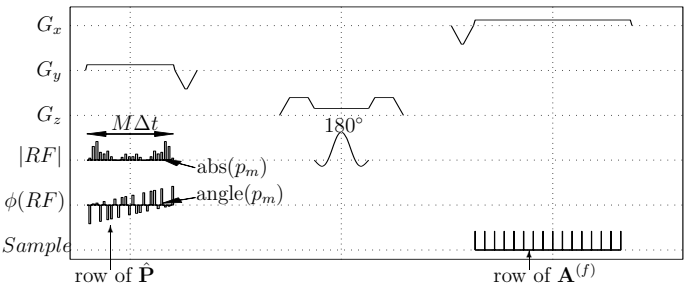

Fig. 1. Timing diagram for a 1D spatial / 1D Fourier encoded spin-echo pulse sequence. The abs(·) and angle(·) functions refer to MATLAB-style notation.

Sensitivity Calibration

A simple approach was used to estimate the spatial sensitivities of each array element based on two full Fourier phase encoded acquisitions of a homogeneous NiCl-doped water phantom using the scanner's body coil and the phased array receivers separately (3). Measured

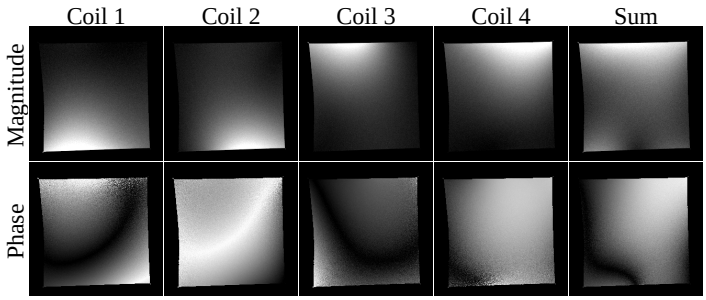

Fig. 2. Spatial coil sensitivities of the elements of the four-element cardiac phased array used in the experiments.

sensitivities are shown in Fig. 2. The intended configuration of the cardiac array elements was used, i.e., two coils anterior (coils 3 & 4), two posterior (1 & 2), each set in a left/right configuration. The same axial plane was used between calibration and accelerated imaging experiments. Array geometry was fixed using a simple Plexiglas enclosure also used for this purpose in clinical P-MRI experiments at our institution. Full phase encoding was achieved using the identity RF encoding matrix (23). Imaging parameters were fixed (TR, TE, BW, etc) for all experiments but sensitivites were acquired for the entire full FOV of 16 cm along both axes. We note that array self-calibration (24) is readily incorporated in our framework by inclusion of the central rows of *k*-space in the subsampling matrix $\mathbf{D}$.

Parallel Imaging Reconstructions

According to the framework presented, any parallel imaging reconstruction method and any set of *k*-space lines can be used to reconstruct the full FOV image. To demonstrate this ability we use Cartesian SENSE and irregularly downsampled Space-RIP.

Cartesian SENSE. A simple Cartesian SENSE (2) implementation with regular integer *k*-space downsampling was used. Tikhonov regularization was used to limit receiver noise in the reconstruction (25).

Irregular Space-RIP. A reduced set of lines to acquire was derived from the *k*-space energy distribution of the imaged sample. In particular, the projection of the *k*-space of the sample onto the readout axis (i.e., norm of each *k*-space line) was assumed to describe a probability mass function (PMF). A series of M/f random numbers drawn according to this PMF immediately yields the set of *k*-space lines used. The Space-RIP system inversion made use of truncated SVD regularization to avoid noise amplification.

Spatial Encoding Methods

Two representative NF encoding methods are used to demonstrate the NF*P framework.

Hadamard Encoding. For M a power of two, the M-by-M Hadamard matrix is defined via the recurrence relation

$$\mathbf{H}_M = \begin{matrix} \mathbf{H}_{M/2} & \mathbf{H}_{M/2} \\ \mathbf{H}_{M/2} & -\mathbf{H}_{M/2} \end{matrix}, \quad \mathbf{H}_2 = \begin{matrix} 1 & 1 \\ 1 & -1 \end{matrix}, \qquad [17]$$

with $\mathbf{H}_2$ the boundary condition. In the low flip-angle approximation, the RF encoding matrix $\hat{\mathbf{P}}$ is derived by Fourier transformation of each row of $\mathbf{H}_M$. The rows of $\hat{\mathbf{P}}$ are then used as RF excitations in consecutive experiment repetitions. A target resolution of $M = 256$ along the NF encoded axis requires use of $\mathbf{H}_{128}$ when a P-MRI speedup of $f = 2$ is used, compared to use of $\mathbf{H}_{256}$ if P-MRI is not applied. Each of the 128 RF pulses derived from $\mathbf{H}_{128}$ is composed of 128 hard pulses, while the sequence produces 256 readout samples from each coil.

For the 4-element array, once all repetitions are completed, the samples are arranged in the 128-by-$(256 * 4)$ composite response matrix $\mathbf{A}^{(f)}$ which then represents the Hadamard spatially encoded FOV contents. Since Hadamard matrices are orthogonal, NF inversion is achieved by multiplying this acquired composite response matrix by the Hermitian conjugate of the RF encoding matrix, i.e., $\hat{\mathbf{P}}^{\dagger} = \hat{\mathbf{P}}^{H}$ in (Eq. [16]). This results in the subsampled composite *k*-space matrix $\mathbf{S}_{\text{est}}^{(f)}$ which is then separated in four pieces, each sized 128-by-256, corresponding to each coil $l = 1, \cdots, 4$. Using the P-MRI method of choice with these reduced-FOV *k*-space matrices directly yields the complex valued image data. The reconstructed image is 256-by-256, while a speedup of 2 is achieved.

Singular Value Decomposition Encoding. Prior to NF imaging, the sample is acquired with the coil array using typical P-MRI phase encoding, yielding four matrices of size 128-by-256. Concatenation of these matrices provides the reference composite system response matrix, $\mathbf{S}^{(f)}$ (i.e., the *a priori* information). The SVD is then calculated as $\mathbf{S}^{(f)} = \mathbf{U}\mathbf{\Sigma}\mathbf{V}^{H}$. Since the matrix $\mathbf{S}^{(f)}$ is 128-by-$(256 * 4)$, $\mathbf{U}$ is 128-by-128, reflecting the P-MRI dimensionality reduction of M/f.

Accelerated SVD encoding is achieved by truncating the SVD vector basis to the first $K \leq M/f$ vectors. The amount of subspace truncation, by retaining K basis vectors, represents the SVD encoding speedup $f_{\text{SVD}} = (M/f)/K$. In this example of $M = 256$ and P-MRI speedup $f = 2$, $f_{\text{SVD}} = 4$ and 8 are obtained by retaining only the first $K = 32$ and 16 columns of $\mathbf{U}$. However, when $f_{\text{SVD}} = 4$ ($K = 32$), the total speedup of the NF*P experiment is in fact $f_{\text{tot}} = M/K = 8$, representing a composite speedup due to the combination of the two methods. This is a rather desirable property as the target speedup may be obtained while neither method is used with an individual speedup that is detrimental to imaging quality.

Use of the K SVD basis vectors from $\mathbf{U}$ for encoding is straightforward. They are directly placed in the rows of $\hat{\mathbf{P}}$ since, in this case, they were computed from a *k*-space reference. For $K = 32$, $\hat{\mathbf{P}}$ is 32-by-128 and each row is used in a sequence repetition. Acquisition and NF inversion proceeds precisely as with Hadamard encoding: readout samples are concatenated to form $\mathbf{A}^{(f)}$, while the rank-K compressed *k*-space approximation of the FOV contents is then reconstructed using Eq. [16]: $\mathbf{S}_{\text{est}}^{(f)} = \hat{\mathbf{P}}^{H}\mathbf{A}^{(f)} = \{\hat{\mathbf{P}}^{H}\hat{\mathbf{P}}\}\mathbf{S}^{(f)}$. This *k*-space estimate is then used with the P-MRI method to reconstruct the image.

RESULTS

Fourier phase and NF encoded P-MRI accelerated experiments were performed using a P-MRI speedup of two, employed along the horizontal direction to reflect coil array element placement (c.f. Fig. 2). Target full FOV matrix size was 256-by-256. All acquisitions used 500 msec TR, 20 msec TE, 10 mm slice thickness, 16 cm FOV gradient for 16 KHz BW along readout. Regular downsampling NF experiments used the compressed RF form $\mathbf{p}^{(f)}$ of length $M/f = 128$ and, for $\Delta t = 20$ μsec, a G_y gradient for 8 cm FOV. Irregular downsampling made use of the full uncompressed form $\mathbf{p}\mathbf{D}^{T}\mathbf{D}$ and a G_y gradient for 16 cm.

Total imaging time for the phase encoded experiments was 64 sec (2x over non P-MRI) in order to acquire the 128 phase encodes. The reconstructed images are shown in the first column of Fig. 3. Results from Hadamard and SVD encoded acquisitions for each P-MRI method are shown in the last 3 columns of Fig. 3. For the P-MRI speedup and target resolution, full encoding of *k*-space also required 128 Hadamard encoding functions, obtained from $\mathbf{H}_{128}$. Imaging time was thus also 64 sec. Truncated SVD encoding offered a combined speedup factor of up to 8x with minimal loss of resolution as shown. For $K = 32$ SVD encoding functions (8x total speedup, third column of Fig. 3), imaging time was 16 sec, while for $K = 16$ (16x total speedup, last column of Fig. 3) imaging time was 8 sec

The results illustrate use of any P-MRI method with any NF encoding method and should not be used for comparing the two particular P-MRI methods. Accordingly, the typical Fourier phase encoded images in the

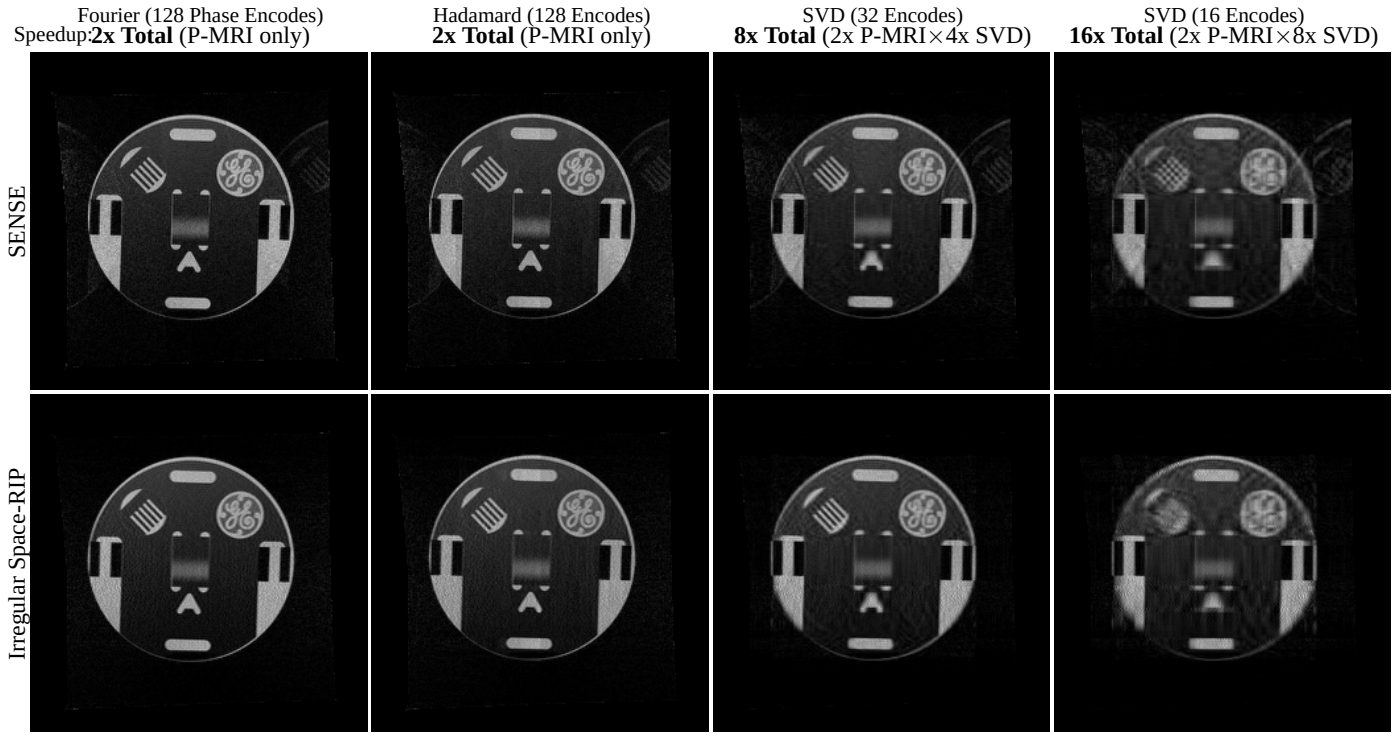

Fig. 3. Fourier P-MRI and non-Fourier P-MRI images acquired using the pulse sequence of Fig. 1. Cartesian SENSE (SENSE) in the top row and irregularly downsampled Space-RIP reconstructions in bottom row. All images are reconstructed to 16 cm FOV and 256-by-256 matrix size and are identically window/leveled. Fourier or non-Fourier encoding and subsequent parallel decoding was applied along the horizontal dimension.

first column of Fig. 3 and their corresponding NF encoded images show that image quality is maintained with NF*P across varying speedup factors for each P-MRI method. The 2x Hadamard and 8x SVD encoded images are similar in quality to their Fourier encoded counterparts. Finally, SVD encoding does not show serious degradation until up to a combined speedup of 16x, bolstering pursuit of this MRI acquisition approach to decrease image acquisition time.

DISCUSSION

The NF*P method allows use of parallel image acquisition in conjunction with non-Fourier encoding. Central to this combination is the proposition of encoding each aliased superimposed portion of the FOV identically. In the language of digital RF encoding, the subsampling of *k*-space employed by P-MRI acquisitions, giving rise to aliasing, is recast as a dimensionality reduction of the digital MR system response matrix that must be encoded. Mathematically then, this dimensionality reduction leads to both fewer as well as shorter RF encoding pulses in the digital RF encoding model.

Resolution along a phase (non-Fourier) encoded dimension is proportional to the number of Fourier (non-Fourier) basis functions. In the digital RF encoding model, both statements express the fact that a column of an image (or, equivalently, *k*-space) matrix with M rows can always be expressed as a combination of precisely M linearly independent basis vectors, whether these vectors are drawn from the Fourier, a Wavelet, or any family of basis functions. P-MRI relaxes this sampling requirement by reducing the FOV by a factor of f while using multiple independent coils to achieve image reconstruction. Easily enough comes the realization that this FOV reduction is equally a matrix size reduction. Digital RF encoding derives a direct correspondence of basis vectors to encoding RF pulses. The FOV is constructed by sampling the linear combinations of basis functions that each column of the FOV is composed of. As a result, the P-MRI FOV reduction allows NF*P to use only M/f RF encoding pulses, thereby manifesting the imaging acceleration of P-MRI.

However, the direct correspondence of basis vector and RF pulse that is the strength of digital RF encoding, is also its foremost limitation. Image resolution along the NF encoded dimension is equal to that of the basis vectors, which in turn is proportional to the length of the RF pulses that are used to excite them. This leads to the second advantage of NF*P: if the basis vectors are only M/f-dimensional, it becomes possible to reduce the length of the RF pulses by a factor up to f, as limited by hardware system constraints.

A Comment on the Use of High Flip-Angle RF Pulses

The NF*P framework uses the low flip-angle approximation to set up the linear equations that enable "digital" RF encoding. Transition to high flip-angle excitations follows by deducing these equations (i.e., the encoding vectors $\mathbf{p}$) directly from the Fourier transform of the desired spatially encoding profiles $\tilde{p}(y)$, rather than specific the RF waveform used to produce these high flip-angle profiles. Once a spatial encoding profile is chosen, the actual RF excitation that produces the profile at any desired flip-angle can be computed (e.g., numerically (26)). Regardless of the specific RF pulse used to induce the profile $\tilde{p}(y)$, multiplication of the spatial domain $\rho(x, y, z)$ and profile in Eq. [3] is equivalent to writing the Fourier transform of the profile within that signal equation. It is then this direct transform of the spatial profile that leads to the linear system and enables use of the matrix equations.

SNR Considerations

The effective Signal-to-Noise Ratio (SNR) of NF*P depends on the SNR of the parallel acquisition as well as that of the particular NF encoding method. The SNR of P-MRI is concisely expressed as (2):

$$SNR^{(f)}(\mathbf{r}) = \frac{SNR^{\text{full}}(\mathbf{r})}{g(\mathbf{r})\sqrt{f}}, \qquad [18]$$

where $SNR^{\text{full}}(\mathbf{r})$ is the SNR attained by full Fourier imaging of the given sample for the given set of acquisition parameters. The factor $1/\sqrt{f}$ is related to the reduction of the FOV by f while maintaining voxel size, while the spatially dependent factor $g(\mathbf{r})$ is related to the conditioning of the numerical inversion problem. The latter is in essence a performance limitation dependent on the ability of the coil ensemble to separate the superimposed aliases at each location in space. When equivalent flip-angle NF encoding replaces phase encoding, Eq. [18] is altered by changing $SNR^{\text{full}}(\mathbf{r})$ with that attained by the particular NF encoding method. This SNR has been studied extensively in e.g., (27), (28) and is affected by a number of factors, viz., similar to the geometry factor $g(\mathbf{r})$ the conditioning of the NF encoding inversion (i.e., Eq.[16]), and, the reduced acquired signal energy stemming from use of an encoding profile that does not make use of all available magnetization.

Hadamard and SVD encoding incur no inversion SNR loss since the encoding matrices are orthogonal. Furthermore, like phase encoding, Hadamard encoding only uses the phase of magnetization for encoding and thus maintains SNR for equivalent flip-angle imaging. However, SVD encoding employs encoding functions that produce variable flip-angle throughout space, hence not all imaged magnetization contributes to each signal acquisition. Intuitive understanding of this SNR loss follows by considering the extreme example of Line Scan encoding which, in the low flip-angle approximation, is achieved by deriving the encoding matrix $\mathbf{P}$ from the Fourier transform of each row of the identity matrix. It is well known that the SNR of Line Scan techniques is reduced by a factor of $1/\sqrt{M}$, when M lines are scanned.

Typical SVD encoding profiles lie somewhere in between these two extreme examples. However, the SNR loss of truncated SVD encoding may not be considerable compared to Fourier imaging if one employs the Rose model (29) to control the subspace truncation (30). In particular, since SVD encoding orders profiles according to expected signal energy (i.e. the singular value), truncation of the encoding vector basis at the point where the expected signal energy falls below the *k*-space noise threshold adds no new information but only noise.

CONCLUSION

The immediate benefit of using the NF*P methodology is enabling P-MRI acceleration for most digital NF encoding MRI modalities, regardless of pulse sequence and encoding method specifics. For example, application of NF*P to volume imaging of the heart (8) can increase the number of slices without increasing imaging time or possibly RF pulse length, or, alternatively, it can be used to reduce imaging time for a given number of slices. Another benefit of NF*P is the ability to combine the static analysis of P-MRI reconstruction with the dynamic analysis offered by near-optimal adaptive NF methods, such as SVD or DATUM (12) encoding, to further reduce acquisition times. The total speedup potentially available to NF*P can exceed that achievable by either encoding method independently.

REFERENCES

1. Sodickson DK, Manning WJ. Simultaneous acquisition of spatial harmonics (SMASH): Fast imaging with radiofrequency coil arrays. Magn Reson Med 1997;38(4):591–603.
2. Pruessmann KP, Weiger M, Scheidegger MB, Boesiger P. SENSE: Sensitivity encoding for fast MRI. Magn Reson Med 1999;42(5):952–962.
3. Kyriakos WE, Panych LP, Kacher DF, Westin CF, Bao SM, Mulkern RV, Jolesz FA. Sensitivity profiles from an array of coils for encoding and reconstruction in parallel (SpaceRIP). Magn Reson Med 2000;44(2):301–308.
4. Kellman P, Epstein FH, McVeigh ER. Adaptive sensitivity encoding incorporating temporal filtering (TSENSE). Magn Reson Med 2001;45:846–852.
5. Madore B. Using UNFOLD to remove artifacts in parallel imaging and in partial-fourier imaging. Magn Reson Med 2002;48(3):493–501.
6. Pruessmann KP, Weiger M, Bornert P, Boesiger P. Advances in sensitivity encoding with arbitrary *k*-space trajectories. Magn Reson Med 2001; 46(4):638–651.
7. Healy Jr DM, Weaver JB. Two applications of wavelet transforms in magnetic resonance imaging. IEEE Trans Information Tech 1992;38(2):840–860.
8. Cunningham CH, Wright GA, Wood ML. High-order multiband encoding in the heart. Magn Reson Med 2002;48:689–698.
9. Panych LP, Zhao L, Jolesz FA, Mulkern RV. Dynamic imaging with multiple resolutions along phase-encode and slice-select dimensions. Magn Reson Med 2001;45(6):940–947.
10. Oh C, Park HW, Cho ZH. Line-integral projection reconstruction (LPR) with slice encoding techniques: Multislice regional imaging in NMR tomography. IEEE Trans Med Imag 1984;MI-3:170–178.
11. Zientara GP, Panych LP, Jolesz FA. Near-optimal encoding for dynamically adaptive MRI: Mathematical principles and computational methods. Int J Imaging Syst and Technol 1999;10:151–165.
12. Hoge WS, Miller EL, Lev-Ari H, Brooks DH, Panych LP. A doubly adaptive approach to dynamic MRI sequence estimation. IEEE Trans Imag Proc 2002;11(10):1168–1178.
13. Healy Jr DM, Weaver JB. Adapted waveform encoding for magnetic resonance imaging. IEEE Engineering in Medicine and Biology 1995; 14(5):621–638.
14. Panych LP, Zientara GP, Jolesz FA. MR image encoding by spatially selective RF excitation: An analysis using linear response models. Int J Imaging Syst and Technol 1999;10:143–150.
15. Hinshaw WS, Lent AH. An introduction to NMR imaging: From the Bloch equation to the imaging equation. In Proc of the IEEE, vol. 71. 1983; 338–350.
16. Strang G. Introduction to Applied Mathematics. Wellesley, Massachusetts: Wellesley-Cambridge Press, 1986; 269–272.
17. Zientara GP, Panych LP, Jolesz FA. Dynamically adaptive MRI with encoding by singular value decomposition. Magn Reson Med 1994; 32(2):268–274.
18. Strang G, Nguyen T. Wavelets and Filter Banks. Wellesley, Massachusetts: Wellesley-Cambridge Press, 1997; 24,32–33.
19. Wang Y. Description of parallel imaging in MRI using multiple coils. Magn Reson Med 2000;44(3).
20. Kyriakos WE, Panych LP. Optimization of SPACE RIP imaging by use of RF selective excitation. In Proc ISMRM Workshop on Minimum Data Acquisition Methods. Florida, USA, 2001; 76–80.
21. Conolly S, Nishimura D, Macovski A, Glover G. Variable-rate selective excitation. J Magn Reson 1988;78:440–458.
22. Mitsouras D. Near real-time 2D dynamic adaptive MRI using near-optimal spatial encoding. In Proc ISMRM Workshop on Minimum Data Acquisition Methods. Florida, USA, 2001; 71–75.
23. Panych LP, Zientara GP, Saiviroonporn P, Yoo SS, Jolesz FA. Digital wavelet-encoded MRI: a new wavelet-encoding methodology. J Magn Reson Imaging 1998;8(5):1135–1144.
24. Jakob PM, Griswold MA, Edelman RR, Sodickson DK. AUTO-SMASH: a self calibrating technique for SMASH imaging. MAGMA 1998;7:42–54.
25. King K. Sense image quality improvement using matrix regularization. In in Proc 9th ISMRM. Glasgow, Scotland, 2001; 1771.
26. Kyriakos WE, Panych LP. Implementation of wavelet encoded MRI with large flip angle pulses. In Proc of the 5th ISMRM. Vancouver, Canada, 1997; 1990.
27. Weaver JB, Healy Jr DM. Signal to noise ratios and effective repetition times for wavelet and adapted wavelet encoding. J of Mag Reson Series A 1995;113:1–10.
28. Panych LP. Theoretical comparison of fourier and wavelet encoding in magnetic resonance imaging. IEEE Trans Med Imag 1996;15(2):141–153.
29. Watts R, Wang Y. *k*-Space interpretation of the Rose model: Noise limitation on the detectable resolution in MRI. Magn Reson Med 2002; 48(3):550–554.
30. Mitsouras D, Edelman AS, Panych LP, Jolesz FA, Zientara GP. Spiral echo-planar trajectories for 3D non-fourier encoded MRI. In in Proc 11th ISMRM. Toronto, Ontario, Canada, 2003; 1009.